DALTON
FULL PAPER

Mononuclear non-heme iron(III) peroxide complexes: syntheses, characterisation, mass spectrometric and kinetic studies †

Alan Hazell,[a] Christine J. McKenzie,*[b] Lars Preuss Nielsen,[b] Siegfried Schindler *[c] and Markus Weitzer[c]

[a] *Department of Chemistry, Aarhus University, 8000 Århus C, Denmark*
[b] *Department of Chemistry, University of Southern Denmark, Odense Campus, 5230 Odense M, Denmark*
[c] *Institute for Inorganic Chemistry, University of Erlangen-Nürnberg, Egerlandstraße 1, 91058 Erlangen, Germany*

Received 30th April 2001, Accepted 29th November 2001
First published as an Advance Article on the web 10th January 2002

A series of transient interconvertible protonated and deprotonated mononuclear Fe(III) peroxo species are derived from the pH dependent reaction of dihydrogen peroxide with mononuclear iron(II) or iron(III) complexes of general formulation $[Fe(Rtpen)X](A)_n$, $n = 1, 2$; X = Cl, Br; Rtpen = *N*-alkyl-*N,N′*,*N′*-tris(2-pyridylmethyl)ethane-1,2-diamine, alkyl = R = CH_3CH_2, $CH_3CH_2CH_2$, $HOCH_2CH_2$, $(CH_3)_2CH$, C_6H_5, and $C_6H_5CH_2$; A = ClO_4, PF_6. The low-spin iron(III) hydroperoxide complex ions $[Fe(Rtpen)(\eta^1\text{-}OOH)]^{2+}$ are purple chromophores and the high-spin iron(III) peroxide complexes, $[Fe(Rtpen)(\eta^2\text{-}OO)]^{+}$ are blue chromophores. The spectroscopic observation (ESR, UV-vis, ESI MS) of a low-spin iron(III) precursor species $[Fe(Rtpen)(\eta^1\text{-}OCH_3)]^{2+}$ and kinetic studies show that formation of $[Fe(Rtpen)(\eta^1\text{-}OOH)]^{2+}$ from iron(II) solution species is a two step process. The first step, the oxidation of the iron(II) complex to $[Fe(Rtpen)(OCH_3)]^{2+}$, is faster than the subsequent ligand substitution during which $[Fe(Rtpen)(\eta^1\text{-}OOH)]^{2+}$ is formed. The kinetic data are consistent with an interchange associative mechanism for the ligand substitution, and a role for the proton bound to the uncoordinated hydroperoxide oxygen atom is suggested. The stability of $[Fe(Rtpen)(\eta^1\text{-}OOH)]^{2+}$ R = $HOCH_2CH_2$, is significantly lower than for the peroxide complexes generated from the other alkyl substituted ligands ($t_{1/2}$ *ca.* 10 min *vs.* several hours). Tandem MS/MS experiments with the $[Fe(Rtpen)(\eta^1\text{-}OOH)]^{2+}$ ions show fragmentation *via* O–O cleavage to give the novel ferryl species $[Fe(Rtpen)(O)]^{2+}$. By contrast the $[Fe(Rtpen)(\eta^2\text{-}OO)]^{+}$ ions are stable under the same gas phase conditions. This indicates a weaker O–O bond in the Fe(III) hydroperoxide complex ions, and that $[Fe^{III}OOH]^{2+}$ rather than $[Fe^{III}OO]^{+}$ species are the precursors to, at least, the ferryl Fe^{IV}=O species. Crystal structures of four starting iron(II) compounds, $[Fe(Rtpen)Cl]PF_6$, R = $HOCH_2CH_2$, $CH_3CH_2CH_2$, $C_6H_5CH_2$, and $[Fe(bztpen)Br]PF_6$ show the iron atoms in distorted octahedral geometries with pentadentate Rtpen coordination with the halide ion as the sixth ligand. The structure of $[Fe(etOHtpen)Cl]PF_6$ shows an intermolecular H-bonding interaction between the dangling hydroxyethyl group and the chloride of a neighbouring molecule with O–H ··· Cl, 3.219(2) Å.

Introduction

Biological mono- and di-nuclear non-heme iron centres are capable of dioxygen activation chemistry to produce oxidants, *e.g.*, Fe peroxide or ferryl species, *etc*.[1,2] The structural characterisation of model complexes with dioxygen/peroxide-derived ligands, and studies of their reactivity, will aid in the detection and elucidation of comparable species formed by non-heme iron biomolecules. These types of compounds are also interesting in their own right as potential new catalysts for the oxidation of organic substrates. To date a mononuclear non-heme Fe(III) peroxide compound has not been isolated, however, several transient mononuclear species have been identified by solution spectroscopy.[3,4] These species are generated either by alkyl- or hydro-peroxide oxidation of mononuclear iron(II) complexes or oxo-bridged diiron(III) systems, and are proposed to contain end-on (η^1) hydroperoxide ligands. Work with dinuclear systems is more advanced: Three dinuclear peroxide-bridged non-heme iron complexes have been characterised by X-ray crystallography.[5]

We have previously reported that a mononuclear iron(II) complex of the pentadentate ligand *N*-methyl-*N,N′*,*N′*-tris(2-pyridylmethyl)ethane-1,2-diamine (metpen, Chart 1), [Fe(metpen)Cl]PF_6, forms a transient purple species when treated with excess H_2O_2 in hydroxylic solvents.[3] The UV-vis and ESR characteristics of this species are comparable to other Fe^{III}–η^1-OOH systems,[4,6] supporting formulation of the purple species as the low-spin Fe(III) hydroperoxo compound $[Fe(metpen)\eta^1\text{-}OOH]^{2+}$. More recently we[6] and Girerd and co-workers[7] independently communicated that $[Fe(metpen)\eta^1\text{-}OOH]^{2+}$ can be deprotonated to give the transient blue complex, $[Fe(metpen)OO]^{+}$. Resonance Raman spectroscopy suggests end-on and side-on coordination respectively for the peroxide ligands in $[Fe(metpen)\eta^1\text{-}OOH]^{2+}$ and $[Fe(metpen)\eta^2\text{-}OO]^{+}$.[8]

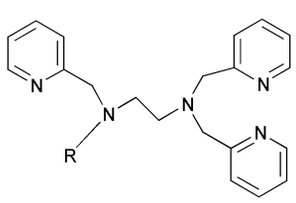

metpen,	R = CH_3
ettpen,	R = CH_3CH_2
etOHtpen,	R = CH_2CH_2OH
prtpen,	R = $CH_3CH_2CH_2$
^{i}prtpen,	R = $(CH_3)_2CH$
phtpen,	R = C_6H_5
bztpen,	R = $CH_2C_6H_5$

Chart 1

† Electronic supplementary information (ESI) available: crystal structures of the cations in $[Fe(^i prtpen)Cl]PF_6$, $[Fe(bztpen)Cl]PF_6$ and $[Fe(bztpen)Br]ClO_4$; rate constants for the reaction of $[Fe(bztpen)Cl](ClO_4)_2$ with H_2O_2. See http://www.rsc.org/suppdata/dt/b1/b103844n/

 DOI: 10.1039/b103844n

The present article describes fully the characterisation of these systems and includes several homologues of the pentadentate ligand system which were prepared in efforts to obtain more stable and therefore potentially isolable iron(III) peroxide adducts. The first detailed kinetic study on formation of a mononuclear non-heme iron(III) peroxide complex, and gas phase formation of a ferryl species, is elaborated.

Experimental

^{1}H and ^{13}C NMR spectra were recorded on 300 MHz Varian Gemini 2000, using $SiMe_4$ as an internal reference. Elemental analyses were performed at the Chemistry Department II at Copenhagen University, Denmark and Atlantic Microlab, Inc., Norcross, Georgia, USA. UV-vis spectra were recorded on a Shimadzu UV-3100 spectrophotometer in CH_3CN. Electrospray ionization (ESI) mass spectra were obtained using a Finnigan TSQ 700 triple quadrupole instrument equipped with a Finnigan API source in the nanoelectrospray mode. Electron spin resonance (ESR) measurements at X-band frequency were obtained using a Bruker ESEMX 113 spectrometer. The related compounds [Fe(tpen)]$(ClO_4)_3$[9] [tpen = *N*-*N*,*N*′,*N*′-tetrakis(2-pyridylmethyl)ethane-1,2-diamine] and Na[Fe(edta)] (edta^{4-} = ethylendiaminetetraacetate) were used to calibrate the low-spin iron(III) and high-spin iron(III) signals respectively. Possible differences in the rates of relaxation for the various iron compounds were eliminated by calibrating at several probe temperatures. The preparation of the iron(II) compounds was carried out using Schlenk techniques, although this precaution may not be strictly necessary. [Fe(metpen)Cl]PF_6[3] and [Fe(bztpen)Cl]$(ClO_4)_2$[9] were prepared as described previously.

Kinetic studies of the reactions of hydrogen peroxide with iron(II)/(III) complexes were performed on a modified Hi Tech SF-3L low temperature stopped-flow unit (Salisbury, UK) equipped with a J&M TIDAS 16-500 diode array spectrophotometer (J&M, Aalen, Germany). Solutions were 2×10^{-4} M in the iron complex and the concentration of the hydrogen peroxide solutions was varied from 0.02 to 0.2 M (pseudo first order conditions ([H_2O_2] ≫ [complex]). Hydrogen peroxide solutions were prepared by adding hydrogen peroxide (30%, titrated with $KMnO_4$) with micropipettes to the methanol solutions (the amount of water was kept constant by adding small amounts of water). Data from the kinetic measurements were either treated with a global analysis fitting routine using the program Specfit (Spectrum Software Associates, Chapel Hill, NC, USA) and/or by extracting single absorbance *vs*. time traces at different wavelengths. These traces were fitted to single exponential functions using the integrated J&M software Kinspec or Igor Pro (WaveMetrics, Lake Oswego, OR, USA).

CAUTION! Although no problems were encountered in the preparation of the perchlorate salts care should be taken when handling such potentially hazardous compounds.

Ligands

All ligands, apart from bztpen,[9] were prepared by the reaction of the appropriate mono-substituted ethylenediamine with three equivalents of 2-chloromethylpyridine hydrochloride in a manner analogous to that described for metpen.[3] The ligands were isolated as yellow oils, apart from bztpen which is a solid, in *ca.* 50–60% yields and were sufficiently pure (NMR) for subsequent complex formation.

Iron(II) complexes

[Fe(Rtpen)Cl]PF_6. $FeCl_2$ (88.7 mg, 0.70 mmol) in 2 ml dry methanol was added to a stirred solution of Rtpen (0.50 mmol), R = CH_3CH_2, $CH_3CH_2CH_2$, $HOCH_2CH_2$, $(CH_3)_2CH$, C_6H_5, or $C_6H_5CH_2$ in 3 ml dry methanol or ethanol containing a few iron turnings. After 15 min NH_4PF_6 (114.1 mg, 0.70 mmol) was added. Diffusion of diethyl ether into the filtered solutions resulted in crystallisation of the yellow product, which was isolated by filtration, washed with diethyl ether and dried under vacuum.

[Fe(ettpen)Cl]PF_6. Yield 65%. Calc. for $C_{22}H_{27}ClF_6FeN_5P$: C, 44.21; H, 4.55; N, 11.72. Found: C, 44,10; H, 4,36; N, 11.55%. λ_{max}/nm (ε/dm^3 mol^{-1} cm^{-1}): 316sh (790), 395 (1760), 920 (13).

[Fe(etOHtpen)Cl]PF_6. Yield 68%. X-Ray quality crystals were grown by diffusion of diethyl ether into a methanolic solution of the complex. Calc. for $C_{22}H_{27}ClF_6FeN_5OP$: C, 43.05; H, 4.43; N, 11.41%. Found: C, 43,34; H, 4,35; N, 11,30%. λ_{max}/nm (ε/dm^3 mol^{-1} cm^{-1}): 321sh (8000), 388 (1700), 895 (20).

[Fe(prtpen)Cl]PF_6. Yield 50%. X-Ray quality crystals were grown by diffusion of diethyl ether into a methanolic solution of the complex. Calc. for $C_{23}H_{29}ClF_6FeN_5P$: C, 45.16; H, 4.78; N, 11.45%. Found: C, 45.47; H, 4.77; N, 11.86%. λ_{max}/nm (ε/dm^{3}mol^{-1}cm^{-1}): 317 (1020), 397 (1950), 916 (14).

[Fe(^{i}prtpen)Cl]PF_6·CH_3CH_2OH. Yield 68%. Calc. for $C_{25}H_{35}ClF_6FeN_5OP$: C, 45.64; H, 5.36; N, 10.65%. Found: C, 46.05; H, 5.44; N, 10.39%. λ_{max}/nm (ε/dm^3 mol^{-1} cm^{-1}): 317sh (780), 392 (1750), 884 (12).

[Fe(phtpen)Cl]PF_6·0.5H_2O. Yield 44%. Calc. for $C_{26}H_{28}ClF_6FeN_5O_{0.5}P$: C, 47.69; H, 4.31; N, 10.70%. Found: C, 47.66; H, 4.13; N, 10.79%. λ_{max}/nm (ε/dm^3 mol^{-1} cm^{-1}): 310sh (882), 390 (2000), 897 (17)

[Fe(bztpen)Cl]PF_6·H_2O. Yield 92%. X-Ray quality crystals were grown by diffusion of diethyl ether into a dichloromethane solution of the complex. Calc. for $C_{27}H_{31}ClF_6FeN_5OP$: C, 47.84; H, 4.61; N, 10.33%. Found: C, 48.17; H, 4.60; N, 9.91%. λ_{max}/nm (ε/dm^3 mol^{-1} cm^{-1}): 320 sh(800), 401 (2050), 891 (17).

[Fe(bztpen)Cl]ClO_4. Reaction as above except that $NaClO_4$·H_2O was added instead of NH_4PF_6. The product precipitated without diffusion of Et_2O. The product was not dried under vacuum. Yield 88%. Calc. for $C_{27}H_{29}Cl_2FeN_5O_4$: C, 52.79; H, 4.75; N, 11.40%. Found: C, 52.70; H, 4.59; N, 11.05%. λ_{max}/nm (ε/dm^3 mol^{-1} cm^{-1}): 322sh (800), 401 (2050), 894 (17).

[Fe(bztpen)Br]ClO_4. $Fe(ClO_4)_3$·$6H_2O$ (83.6 mg, 0.236 mmol) was added to a solution of Et_4NBr (200 mg, 0.952 mmol) in 3 ml dry MeOH. Bztpen (100 mg, 0.236 mmol) in 3 ml dry MeOH was added and the red solution was allowed to crystallise over night. The brown crystals were isolated by filtration. Yield 69%. Calc. for $C_{27}H_{29}BrClFeN_5O_4$: C, 49.23; H, 4.44; N, 10.63%. Found: C, 49.25; H, 4.50; N, 10.69%. λ_{max}/nm (ε/dm^3 mol^{-1} cm^{-1}): 317sh (820), 394 (2250), 934 (10)

[Fe(bztpen)Cl]$(PF_6)_2$. $FeCl_3$·$6H_2O$ (63.8 mg, 0.236 mmol) in dry MeOH (1 ml) was added to a solution of bztpen (100 mg, 0.236 mmol) in dry MeOH (2 ml). A yellow precipitate formed immediately and redissolved spontaneously after *ca.* 2 min. Addition of NH_4PF_6 resulted in precipitation of the yellow product, which was isolated by filtration. Yield 89 mg, 47%. Calc. for $C_{27}H_{29}ClF_{12}FeN_5P_2$: C, 40.30; H, 3.63; N, 8.70%. Found: C, 40.54; H, 3.78; N, 8.69%. λ_{max}/nm (ε/dm^3 mol^{-1} cm^{-1}): 302 sh (5800), 368 (4000).

X-Ray crystallography

Crystal data and details of the structure determination for [Fe(etOHtpen)Cl]PF_6, [Fe(^{i}prtpen)Cl]PF_6·0.5C_4H_{10}, [Fe(bztpen)Cl]PF_6·0.192CH_2Cl_2 and [Fe(bztpen)Br]ClO_4 are given in Table 1. Data were collected on a Siemens SMART diffractometer with a CCD area detector with graphite monochromatised MoKα radiation, the crystals were cooled to 120 K using a cryostream nitrogen gas cooler system.[10] Programs used for

Table 1 Crystal data and structure refinements

	[Fe(etOHtpen)Cl]PF_6	[Fe(prtpen)Cl]PF_6·0.5$C_4H_{10}O$	[Fe(bztpen)Cl]PF_6·0.192CH_2Cl_2	[Fe(bztpen)Br]ClO_4
Empirical formula	$C_{22}H_{27}N_5OF_6PClFe$	$C_{25}H_{34}N_5O_{0.5}F_6PClFe$	$C_{27.192}H_{29.384}N_5F_6PCl_{1.384}Fe$	$C_{27}H_{29}N_5O_4BrClFe$
Formula weight	613.78	648.87	676.16	658.79
Crystal system	Orthorhombic	Triclinic	Rhombohedral	Orthorhombic
Space group	*Fdd*2	$P\bar{1}$	$R\bar{3}$	*Pbca*
a/Å	21.345(1)	8.7288(4)	29.150(1)	16.6209(7)
b/Å	53.473(3)	12.3068(6)	29.150(1)	17.8973(8)
c/Å	9.0756(5)	13.5844(6)	17.661(1)	18.1065(8)
α/°	90	100.215(1)	90	90
β/°	90	96.395(1)	90	90
γ/°	90	94.920(1)	120	90
V/Å^3	10359(1)	1418.9(1)	12996(1)	5386.1(4)
Z	16	2	18	8
D_{calc}/g cm^{-3}	1.574	1.519	1.555	1.625
T/K	120	123	120	120
μ(MoKα)/mm^{-1}	0.813	0.745	0.772	2.191
Crystal size/mm	0.36 × 0.28 × 0.12	0.50 × 0.24 × 0.14	0.44 × 0.40 × 0.34	0.50 × 0.40 × 0.20
θ range/°	2.1–28.6	2.5–29.7	2.4–29.84	2.0–29.8
Reflections collected	16435	10123	42461	67942
independent (R_{int})	5618(0.039)	6520(0.025)	7899(0.042)	7728(0.066)
observed [$I > 2\sigma I$]	5399	5945	6787	6422
Absorption correction	Integration	Integration	Integration	Integration
Transmission	0.735–0.911	0.711–0.916	0.766–0.886	0.391–0.646
Refinement method	Full-matrix least-squares on *F*			
Data/constraints/parameters	5399/0/338	5945/0/379	6787/6/387	6422/0/353
R indices[a] [$I > 2\sigma I$] *R*1	0.027	0.029	0.046	0.028
*wR*1	0.037	0.038	0.037	0.033
A, *B*	0.03, 0.20	0.03, 0.20	0.03, 7.0	0.03, 0.10
$\Delta\rho_{max}$, $\Delta\rho_{min}$/e Å^{-3}	0.60(8), −0.48(8)	0.47(6), −0.39(6)	1.1(1), −1.1(1)	0.64(7), −0.43(7)

[a] $R1 = \Sigma\big||F_o| - |F_c|\big|/\Sigma|F_o|$. $wR1 = (\Sigma w(|F_o| - |F_c|)^2/\Sigma wF_o^2)^{1/2}$. $w = 1/\{(\sigma(F_o^2) + B + (1 + A)F_o^2)^{1/2} - |F_o|\}^2$.

data collection, data reduction and absorption correction were SMART,[11] SAINT[11] and XPREP.[11] The structures were solved by direct methods, using SIR97,[12] and structures were refined on *F* using the modification ORFLS[13] in KRYSTAL,[14] hydrogen atoms were constrained to chemically reasonable positions with $U_{iso} = 1.2U_{eq}$ for the atoms to which they were attached, except for the hydroxyl hydrogen atom of [Fe(etOHtpen)Cl]PF_6 which was located from a difference map and refined isotropically. A difference map for [Fe(bztpen)Cl]PF_6 showed peaks in a channel running parallel to the *c*-axis, these were interpreted as a partially occupied CH_2Cl_2 site. Atomic scattering factors were from ref. 15. Selected bond distances and angles are given in Table 2.

CCDC reference numbers 163870–163873.

See http://www.rsc.org/suppdata/dt/b1/b103844n/ for crystallographic data in CIF or other electronic format.

Results and discussion

Syntheses and X-ray crystal structures

The ligands (generic name Rtpen) *N*-methyl-*N,N′,N′*-tris(2-pyridylmethyl)ethane-1,2-diamine (metpen), *N*-ethyl-*N,N′,N′*-tris(2-pyridylmethyl)ethane-1,2-diamine (ettpen), *N*-hydroxyethyl-*N,N′,N′*-tris(2-pyridylmethyl)ethane-1,2-diamine (etOHtpen), *N*-propyl-*N,N′,N′*-tris(2-pyridylmethyl)ethane-1,2-diamine (prtpen), *N*-isopropyl-*N,N′,N′*-tris(2-pyridylmethyl)ethane-1,2-diamine (^{i}prtpen), *N*-phenyl-*N,N′,N′*-tris(2-pyridylmethy)ethane-1,2-diamine (phtpen) and *N*-benzyl-*N,N′,N′*-tris(2-pyridylmethyl)ethane-1,2-diamine (bztpen), are shown in Chart 1. Metpen and bztpen have been reported earlier.[3,6] The yellow crystalline iron(II) and iron(III) complexes of general formulation [Fe(Rtpen)X](A) and [Fe(Rtpen)Cl](A)$_2$, X = Cl, Br, A = ClO_4 or PF_6 are prepared by the stoichiometric reaction of each ligand with the appropriate iron salt in dry methanol followed by the addition of a salt of the counter anion. All ESI mass spectra of the complexes show the iron(II) complex, [Fe(Rtpen)Cl]$^+$, as base peak, regardless of initial oxidation state, however iron(III) species are present in the ESI mass spectra of [Fe(bztpen)Cl](A)$_2$, A = PF_6 or ClO_4. The iron(III) complexes are unstable in solutions that are not completely free of water: the hydrolysis product, the orange μ-oxo-bridged iron(III) compound [(bztpen)ClFe(μ-O)FeCl(bztpen)](A)$_2$, can be isolated from aged solutions of [Fe(bztpen)Cl](A)$_2$. This oxo-bridged diiron(III) complex (characterised by ESI MS, IR, UV-vis and elemental analysis) is expected to show a cation structure analogous to that of [(metpen)ClFe(μ-O)FeCl(metpen)]$^{2+}$.[16] The bromide complex [Fe(bztpen)Br]PF_6 was obtained from a reaction containing Fe(III), however the Fe(III) species is apparently reduced by bromide and the product isolated was an iron(II) complex.

Table 2 Selected bond distances [Å] and angles [°]

	1 (X = Cl)	**2** (X = Cl)	**3** (X = Cl)	**4** (X = Br)
Fe–X	2.363(1)	2.3717(4)	2.325(1)	2.4801(3)
Fe–N1	2.257(2)	2.297(1)	2.248(2)	2.223(1)
Fe–N4	2.271(2)	2.323(1)	2.251(2)	2.265(1)
Fe–N11	2.174(2)	2.207(1)	2.177(2)	2.166(1)
Fe–N21	2.212(2)	2.201(1)	2.227(2)	2.206(1)
Fe–N31	2.243(2)	2.175(1)	2.276(2)	2.271(1)
X–Fe–N1	165.57(5)	159.52(3)	167.77(5)	171.38(4)
X–Fe–N4	110.64(5)	117.15(3)	102.13(5)	102.42(4)
X–Fe–N11	100.56(5)	94.55(4)	109.04(5)	106.54(4)
X–Fe–N21	92.78(5)	90.31(3)	92.42(5)	94.89(4)
X–Fe–N31	91.62(5)	92.89(3)	92.72(5)	90.48(4)
N1–Fe–N4	79.40(6)	77.95(4)	79.63(6)	79.53(5)
N1–Fe–N11	74.09(7)	74.55(5)	73.97(7)	75.09(5)
N1–Fe–N21	75.25(6)	75.95(5)	75.38(7)	76.53(5)
N1–Fe–N31	101.28(7)	104.65(5)	99.40(7)	98.11(5)
N4–Fe–N11	143.50(6)	146.49(5)	143.46(7)	143.87(5)
N4–Fe–N21	97.39(6)	87.58(5)	99.90(7)	95.39(5)
N4–Fe–N31	74.47(6)	76.38(5)	74.91(6)	73.92(5)
N11–Fe–N21	99.58(7)	103.72(5)	97.39(7)	103.09(5)
N11–Fe–N31	86.50(6)	92.37(5)	84.87(6)	84.60(5)
N21–Fe–N31	171.71(7)	163.30(5)	173.37(7)	168.89(5)

The crystal structures of the cations in [Fe(etOHtpen)Cl]PF_6, [Fe(^{i}prtpen)Cl]PF_6, [Fe(bztpen)Cl]PF_6 and [Fe(bztpen)Br]ClO_4, are similar. That for [Fe(etOHtpen)Cl]PF_6 is shown in Fig. 1.

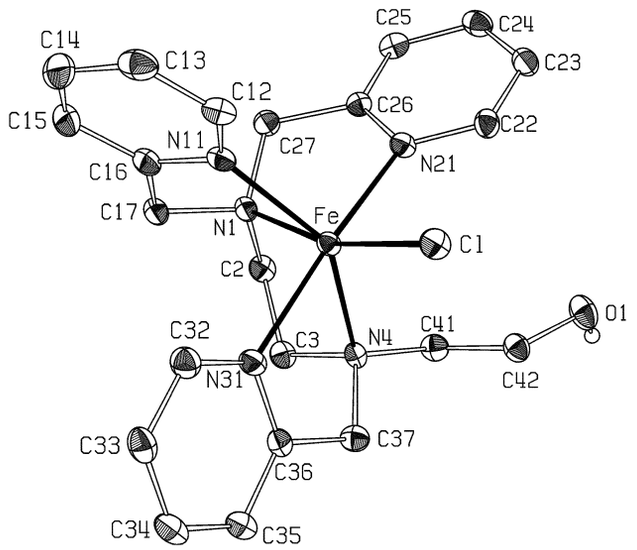

Fig. 1 Thermal ellipsoid drawing of $[Fe(etOHtpen)Cl]PF_6$ with 50% probability, showing the atom numbering scheme.

Figures of the remaining structures are included in the ESI.† Selected bond distances and angles are listed in Table 2. The iron atoms in all of the structures show distorted octahedral geometries. The faces containing the halide ligands are relatively open with all of the angles to donor nitrogen atoms *cis* to the halide significantly greater than 90°. The crystal structures suggest that the pentadentate Rtpen ligands provide, on coordination to an iron atom, a relatively open face which may be suitable for housing not only single terminal ligands like chloride but also small diatomic side-on bound molecules like η^2-OO, as proposed below. The pendant ethylhydroxyl group in the structure of $[Fe(etOHtpen)Cl]^+$ is intramolecularly H-bonded to the chloride ligand of an adjacent molecule with an O ··· Cl distance of 3.219(2) Å.

Reactivity towards H_2O_2: generation of the purple and blue chomophores

The reactions of all of the complexes with an excess (*ca.* 300 equivalents) of dihydrogen peroxide generated purple solutions with spectroscopic characteristics similar to those we reported[3] for the parent $[Fe(metpen)(\eta^1\text{-}OOH)]^{2+}$ in hydroxylic solvents. Analogous low-spin Fe(III) hydroperoxide chromophores containing end-on bound hydroperoxide ligands are proposed for the new, related compounds, $[Fe(Rtpen)(\eta^1\text{-}OOH)]^{2+}$, R = CH_3CH_2, $CH_3CH_2CH_2$, $HOCH_2CH_2$, $(CH_3)_2CH$, C_6H_5, and $C_6H_5CH_2$. An excess of peroxide is needed because of the reversibility of the reaction, *vide infra*. Except for solutions derived from $[Fe(etOHtpen)Cl]PF_6$, the purple solutions are stable for several hours at ambient temperature. The purple chromophore assigned to $[Fe(etOHtpen)(\eta^1\text{-}OOH)]^{2+}$ is observed only for approximately 10 min under the same conditions. Formation of the purple hydroperoxide species is instantaneous when the new iron(III) starting compounds, $[Fe(bztpen)Cl](A)_2$, A = ClO_4, PF_6, are used in reactions with hydrogen peroxide. By contrast, there is a time lag of a few seconds before the appearance of the purple colour when the iron(II) starting materials are used. This time lag is caused by the necessary oxidation of the iron(II) complex to the low-spin iron(III) intermediate $[Fe(Rtpen)(OCH_3)]^{2+}$ prior to the reaction with hydrogen peroxide. We have identified the ESR signal due to $[Fe(Rtpen)(OCH_3)]^{2+}$ generated by the alternative method of exchange of the chloride ion in $[Fe(bztpen)Cl](ClO_4)_2$ for methoxide.[9] A reaction scheme for the formation of the peroxide complexes is presented in Scheme 1. The purpose in preparing the present series of new ligands based on simple modifications of the same basic framework as metpen,[3] was to tune the solubility, and stability, of the transient Fe(III) peroxo species, with the intention of solid state isolation. Unfortunately it seems that no significant stabilisation was attained, indeed, as mentioned above, the hydroperoxo complex based on etOHtpen decomposes significantly faster than the others. A plausible explanation is that an intramolecular H-bonding arrangement of the type depicted in Chart 2 destabilises the hydroperoxide

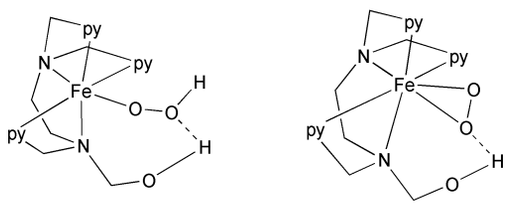

Chart 2

complex by weakening the O–O and/or Fe–O bond of the peroxide ligand with the consequence of accelerating the decomposition of the peroxide species. The original rationale behind the preparation of etOHtpen was in fact an attempt to create a situation suitable for an intramolecular H-bonding interaction between the hydroperoxide ligand and the non-coordinated etOHtpen hydroxyl group in $[Fe(etOHtpen)(\eta^1\text{-}OOH)]^{2+}$.

The addition of 30 equivalents of ammonia, triethylamine or pyridine to the purple solutions of $[Fe(Rtpen)(\eta^1\text{-}OOH)]^{2+}$ produce a transient blue colour. If the base is first added to methanolic solutions of $[Fe(Rtpen)Cl]^+$ followed by hydrogen peroxide the blue solution is generated directly. Subsequent addition of hydrochloric acid to the blue solutions regenerates the purple one. This cycle can be repeated several times with the same solution indicating a reversible acid/base equilibrium. The spectroscopic evidence suggests that the blue species are novel $[Fe^{III}(Rtpen)OO]^+$ species derived from the deprotonation of $[Fe(Rtpen)OOH]^{2+}$. Alternative dinuclear structures for the blue species, *e.g.*, $[(Rtpen)Fe(\mu,\eta^2\text{:}\eta^2\text{-}O_2)Fe(Rtpen)]^{4+}$, can be discounted on the basis of ESI MS and ESR spectroscopy. The maxima in the visible region of the electronic spectrum are

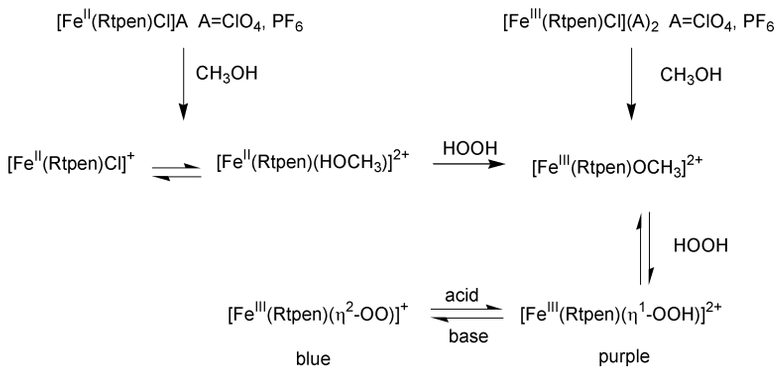

Scheme 1

Table 3 Comparison of visible spectroscopy data for transient purple Fe(III) hydroperoxide and blue Fe(III) peroxide species derived from $[Fe(Rtpen)]^{3+}$. Recorded in methanol. Extinction coefficients are not listed since the concentrations of peroxide species cannot be determined

Starting complex	Purple species, λ_{max}/nm	Blue species, λ_{max}/nm
$[Fe(metpen)Cl]PF_6$	536	748
$[Fe(ettpen)Cl]PF_6$	536	747
$[Fe(etOHtpen)Cl]PF_6$	537	716
$[Fe(prtpen)Cl]PF_6$	539	771
$[Fe(^{i}prtpen)Cl]PF_6$	538	753
$[Fe(bztpen)Cl]PF_6$	542	770

around 536 nm and 750 nm respectively for the purple and blue species. The λ_{max} for the peroxide to iron(III) charge-transfer bands are listed in Table 3. The difference in the maxima is consistent with the expected increased donor strength of the O_2^{2-} *vs.* O_2H^- ligand. However, this simple argument is complicated by a concomitant spin change of the iron atom (see ESR results below). Notably the O^{2-}–Fe^{III} CT band recorded for $[Fe(etOHtpen)OO]^+$ occurs at the lowest wavelength for the $[Fe(Rtpen)OO]^+$ species. This attenuation could be consistent with a weakening of the ligand field through a hydrogen bonding interaction of the pendant uncoordinated hydroxyethyl arm of etOHtpen to an oxygen atom of the peroxide ligand (Chart 2).

Girerd and co-workers have recently reported the resonance Raman spectra of the purple and blue metpen-derived hydroperoxide and peroxide species.[8] Bands at 620 and 800 cm^{-1} were assigned to Fe–O and O–O stretching modes respectively for the hydroperoxo complex with bands at 465 and 820 cm^{-1} corresponding to the stretching modes for the blue peroxo complex. On this basis it is reasonable to assume an η^1 coordination geometry for the hydroperoxide ligand and η^2 coordination geometry for the peroxide ligand. Given the similarity of the other spectroscopic data for the present series we believe their structures to be analogous to those of the parent metpen compounds. One question remaining is the coordination number of the iron(III), in particular for the deprotonated peroxide complexes, $[Fe(Rtpen)OO]^+$. Both 6- and 7-coordination are feasible, the former if one of the picolyl arms is uncoordinated. The example of a non-heme-peroxo complex which has been known for 30 years, $[Fe(edta)O_2]^{3-}$ is proposed to contain a side-on (η^2) peroxide ligand and 6-coordinated iron(III).[17,18]

Detection of Fe^{III}–OOH, Fe^{III}–OO and a Fe^{IV}=O species by ESI MS

Consistent with an acid/base equilibrium, peaks assigned to both the protonated and deprotonated Fe(III) peroxide complexes, $[Fe(Rtpen)OOH]^+$ and $[Fe(Rtpen)OO]^{2+}$ are observed in the ESI mass spectra of the purple and blue solutions in methanol or ethanol. Also, the starting iron(II) complexes, $[Fe(Rtpen)Cl]^+$, and ions containing deprotonated solvent instead of chloride were detected. Fluorinated cations, $[Fe(Rtpen)F]^+$, were present in the spectra of the hexafluorophosphate salts. The following results for the bztpen system exemplifies the series: Fig. 2 shows a spectrum of the purple solution generated from the reaction of $[Fe(bztpen)Cl]PF_6$ with dihydrogen peroxide in ethanol. No direct relationship between the concentration of complex, hydrogen peroxide and base and the intensity of the peaks in the ESI mass spectra is possible, but a trend was noted: The ratio between *m/z* 256.1 and 511.2 ions corresponding to $[Fe(bztpen)OOH]^{2+}$ and $[Fe(bztpen)OO]^+$ respectively, increases in the spectra of the blue solutions. Interestingly a prominent peak (often the most intense) at *m/z* 247.6 can be assigned to a ferryl species formulated as $[Fe(bztpen)O]^{2+}$. The isotopic pattern shows that the ion is doubly-charged, eliminating an alternative assignment of a

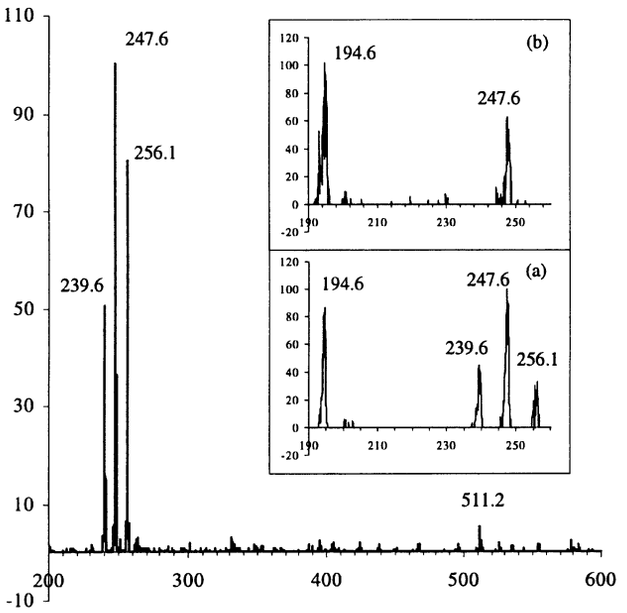

Fig. 2 The electrospray ionisation mass spectrum of the purple solution generated by the reaction of $[Fe(bztpen)Cl](ClO_4)_2$ with 1000 equivalents of hydrogen peroxide in ethanol. Inserts: CID spectra of (a) the *m/z* 256.1 ion, (b) the *m/z* 247.6 ion. Assignments: *m/z* 256.1, $[Fe(bztpen)(OOH)]^{2+}$; 511.3, $[Fe(bztpen)(OO)]^+$; 247.5, $[Fe(bztpen)O]^{2+}$; 239.5, $[Fe(bztpen)]^{2+}$; 194.5, $[Fe(bztpen\text{-}C_7H_6)]^{2+}$.

peroxo-bridged dimer with the same stoichiometry, *i.e.*, $[(bztpen)Fe(O_2)Fe(bztpen)]^{4+}$. Additional structural information is obtained from tandem mass spectrometry (MS/MS) experiments. Collision induced dissociation (CID) of the ion at *m/z* 256.1 produces *m/z* 247.6, 239.6 and 194.6 ions. Thus the *m/z* 247.6 ion can be explained by hydroxyl radical loss from $[Fe(bztpen)(OOH)]^{2+}$. The *m/z* 239.6 ion is assigned to $[Fe(bztpen)]^{2+}$, by loss of the hydrosuperoxide radical from $[Fe(bztpen)(OOH)]^{2+}$. The third peak is assigned to a species in which the hydroperoxide group and a dangling alkyl group of the ligand have been removed, $[Fe(bztpen - C_7H_6)]^{2+}$. In order to determine whether or not the peaks at *m/z* 239.6 and 194.6 can result from fragmentation of the *m/z* 247.6 ion ($[Fe(bztpen)O]^{2+}$) as well as, or rather than the hydroperoxide ion, $[Fe(bztpen)OOH]^{2+}$, a MS/MS experiment on the *m/z* 247.6 ion was performed. This resulted in the generation of the *m/z* 194.6 ion only. Thus the oxygen atom is lost only together with the dangling alkyl group. Thus loss of 106 mass units from $[Fe(bztpen)O]^{2+}$ can be ascribed to loss of the mass equivalent to benzaldehyde. Intramolecular oxo transfer from the ferryl to the dangling benzyl to generate benzaldeyde *via* an oxidative cleavage of bztpen seems a plausible route. The iron(II) species which is expected to remain after benzaldehyde loss, $[Fe^{II}(bztpen - C_7H_6)]^{2+}$ (= $\{[Fe^{IV}(bztpen)O] - C_7H_6O\}^{2+}$) fits with observation of the *m/z* 194.6 ion. By contrast, the CID spectrum obtained under similar conditions of the *m/z* 511.2 ion ($[Fe(bztpen)O_2]^+$) does not show any of the peaks assignable to $[Fe^{IV}(bztpen)O]^{2+}$. A summary of the processes is depicted in Scheme 2. A similar set of ESI MS results were obtained for the other members of the series: A ferryl species $[Fe(Rtpen)O]^{2+}$ was observed and its CID spectrum showed mass losses equivalent to the appropriate aldehyde, RCHO. The potential of the skimmer region was varied to check whether the putative gas phase ferryl ion is also present in solution, however the results were not conclusive.

The comparative ease of O–O (and Fe–O) bond cleavage in $[Fe(Rtpen)OOH]^{2+}$ compared with $[Fe(Rtpen)OO]^+$ observed in the MS/MS experiments is in agreement with the expectation that Fe(III) hydroperoxide species are more likely to undergo O–O bond cleavage to give highly reactive ferryl oxidants, compared to their (side-on bound) peroxide counterparts. A

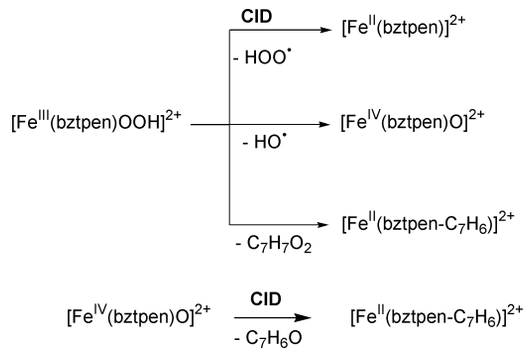

Scheme 2

similar pathway to the formation of the highly oxidising ferryl species thought responsible for oxidative DNA damage in iron bleomycin has been suggested, *i.e.*, the FeO–OH bond in the spectroscopically identified iron(III) hydroperoxide species, "activated" bleomycin (BLM), cleaves to give either Fe^{IV}=O or Fe^{V}=O species.[2]

Reactions of Fe–Rtpen complexes with other oxidants

The Fe–OOH, Fe–OO and Fe=O species are not artifacts that can be generated by reacting the iron complexes with oxidants other than dihydrogen peroxide. Addition of a large excess (up to 1000 fold) of *tert*-butylperoxide or bromine to solutions (methanol, ethanol, acetonitrile, acetone, water) of [Fe(Rtpen)-Cl]PF_6 or [Fe(bztpen)Cl]$(ClO_4)_2$ did not lead to purple/blue solutions or detectable formation (ESI MS) of the above mentioned peroxide, oxide or alkylperoxo iron complexes. However the complexes are oxidised since iron(III) species containing deprotonated solvent, $[Fe(Rtpen)OH]^{2+}$ and $[Fe(Rtpen)-OCH_3]^{2+}$ from water and methanol respectively, and in addition, $[Fe(Rtpen)Br]^{2+}$ from solutions containing bromine, dominate the ESI mass spectra.

ESR spectroscopy

Starting compounds, [Fe(Rtpen)Cl](PF_6) and [Fe(Rtpen)-Cl]$(PF_6)_2$. The high-spin iron(II) starting materials [Fe(Rtpen)-Cl]A, A = ClO_4, PF_6, are as expected ESR silent. A high-spin Fe(III) signal (g = 8.0, 5.7, 4.4) is observed for [Fe(bztpen)-Cl]$(A)_2$, A = ClO_4, PF_6, in the solid state. In methanol solution at 100 K, a rhombic low-spin signal (g = 2.32, 2.14, 1.93) is present in the spectra of the Fe(III) complexes (Fig. 3a). This signal is assigned not to the chloride complex as for the solid state, but rather the methoxide complex $[Fe(Rtpen)OCH_3]^{2+}$.[9] Addition of equimolar amounts of hydrogen peroxide to methanolic solutions of the iron(II) complexes [Fe(Rtpen)Cl](PF_6) produces the same low-spin signal due to $[Fe(Rtpen)OCH_3]^{2+}$. The signal due to $[Fe(Rtpen)OCH_3]^{2+}$ eventually disappears on addition of water. This is due to hydrolysis and formation of the μ-oxo complex [(bztpen)ClFe(μ-O)FeCl(bztpen)]$(PF_6)_2$ which could be isolated. The data obtained for all the compounds were the same regardless of the R group on the ligand.

Peroxide complexes. The ESR studies of the bztpen systems (Fig. 3) exemplify the observations made for all the systems: Spectra of the purple solutions generated from the reaction of [Fe(bztpen)Cl]$(PF_6)_n$, n = 1, 2, with approximately 100 equivalents of hydrogen peroxide show two overlapping rhombic signals indicative of the two low-spin Fe(III) species $[Fe(bztpen)(\eta^1\text{-}OOH)]^{2+}$ (g = 2.20, 2.16, 1.96) and its precursor, $[Fe(bztpen)OCH_3]^{2+}$ (g = 2.32, 2.14, 1.93) as depicted in Scheme 1 (Fig. 3b). That formation of the peroxide compounds from the iron(II) species proceeds *via* the low-spin iron(III) methoxide intermediate followed by reversible ligand exchange was confirmed by the results of the kinetic study detailed below. Notably stoichiometric amounts of hydrogen peroxide were

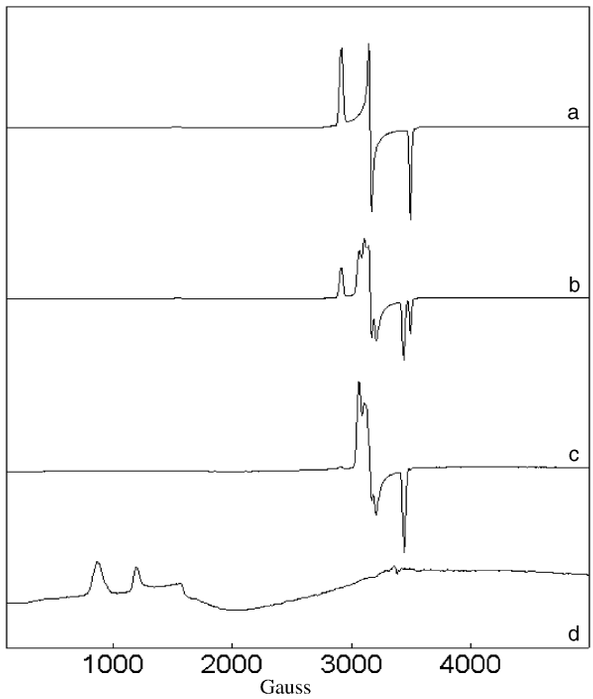

Fig. 3 (a) ESR spectra $[Fe^{III}(ettpen)Cl](PF_6)_2$ dissolved in methanol, the signal observed is due to $[Fe^{III}(ettpen)OCH_3]^{2+}$ (g = 2.32, 2.14, 1.93). (b) Addition of 100 equivalents of 35% H_2O_2 to $[Fe^{III}(ettpen)OCH_3]^{2+}$, a new signal due to $[Fe^{III}(ettpen)(\eta^1\text{-}OOH)]^{2+}$ (g = 2.20, 2.16, 1.96) grows in (solution still yellow). (c) After the addition of excess (300 equivalents) of 35% H_2O_2 to give a purple solution due to $[Fe^{III}(ettpen)(\eta^1\text{-}OOH)]^{2+}$. (d) Blue solution generated after addition of 30 equivalents of triethylamine. The spectrum shows an iron(III) high-spin signal at g = 7.60 and 5.74 assigned to $[Fe^{III}(ettpen)OO]^+$.

sufficient to oxidise the iron(II) complex to its corresponding iron(III) complex, whereas a large excess was necessary to produce the Fe(III) hydroperoxide complex; the more dihydrogen peroxide added the higher the proportion of the hydroperoxide complex observed. The addition of *ca.* 300 equivalents of hydrogen peroxide produces the spectrum in Fig. 3c which now shows that the low-spin $[Fe(bztpen)(\eta^1\text{-}OOH)]^{2+}$ dominates. Addition of 30 equivalents of base to give the blue solutions results in new signals at g = 7.60 and 5.74 due to the formation of a high-spin iron(III) species (Fig. 3d). A high spin iron(III) impurity causes the peak at g = 4.3.[19] Correlation of the UV-vis and ESR spectra showed a direct relationship between the concentration of the high-spin species in the ESR spectra and the intensity of the *ca.* 750 nm band, confirming that the high-spin signals detected by ESR spectroscopy are with certainty due to the blue chromophores.

The ESR signals were calibrated in order to make an estimation of the percentage conversion in the reactions with hydrogen peroxide (shown in Scheme 1). 100% of the iron(II) species $[Fe(bztpen)Cl]^+$ can be converted to the low-spin iron(III) species $[Fe(bztpen)OCH_3]^{2+}$ and $[Fe(bztpen)OOH]^{2+}$ (relative amounts of each iron(III) product depending on the H_2O_2 excess); 25% of the low-spin $[Fe(bztpen)OOH]^{2+}$ can be converted to the high-spin signal assigned to $[Fe(bztpen)OO]^+$. The apparent incomplete conversion is accounted for by the competing equilibrium reactions, with the iron(II) species favoured. Ultimately the iron(III) species decompose to ESR silent oxo-bridged dimers. These have both been isolated, and characterised and detected by ESI MS ($[(bztpen)ClFe-(\mu\text{-}O)FeCl(bztpen)]^{2+}$ at m/z 522) and from hydrogen peroxide treated solutions of the complexes.

Kinetic studies

To gain a better understanding of the reactions of the iron(II) and iron(III) complexes with hydrogen peroxide we have investi-

gated these reactions by stopped-flow techniques. A detailed kinetic study has allowed elucidation of the mechanism of these reactions.

The reaction of H_2O_2 with the iron(III) complex, [Fe(bztpen)-Cl](ClO$_4$)$_2$. The reaction of the iron(III) complex [Fe(bztpen)-Cl](ClO$_4$)$_2$ with a large excess of hydrogen peroxide in methanol can be observed spectrophotometrically, and time resolved spectra of the formation of the peroxo complex are shown in Fig. 4. Absorbance *vs*. time data in the wavelength range

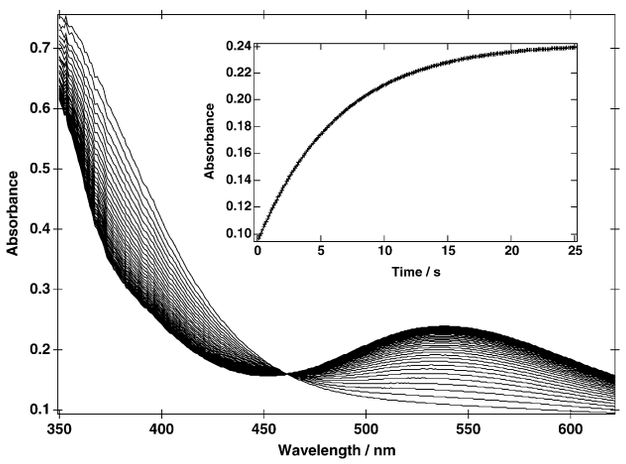

Fig. 4 Time resolved UV-vis spectra of the reaction of [Fe(Bztpen)-Cl](ClO$_4$)$_2$ with hydrogen peroxide in methanol (30.0 °C, [complex] = 0.2 mM, [H_2O_2] = 0.1 M). Insert: absorbance *vs*. time trace at 550 nm (data: +, fit to one exponential function: —).

between 475 nm and 620 nm could be fitted to one exponential function. The insert in Fig. 4 shows the measured data as well as the excellent calculated fit at 540 nm. All data are listed in Table S1 (ESI).† This was not the case for data obtained from the wavelengths to the left of the isosbestic point in Fig. 4. Here it was necessary to fit the data to the sum of two exponentials. One of the rate constants was identical to the one obtained from the fit at higher wavelengths. The small spectral changes caused by the second reaction, observed at wavelengths below 450 nm, are associated with dilution of the complex by methanol (which contains water), both with and without hydrogen peroxide. This second reaction is most likely caused by reaction of the mononuclear complex, *e.g.*, μ-oxo-bridged dimer formation and will not be discussed further. A variation of the concentration of hydrogen peroxide from an excess of 100 to 500 compared to the complex at different temperatures (−10 to +30 °C) leads to straight lines with an intercept in a plot of the observed rate constants *vs*. [H_2O_2]. The intercept is a consequence of the reversibility of the reaction and it is necessary to use a large excess of hydrogen peroxide to shift the equilibrium to the product side. From the slopes, second order rate constants (see Table 4) for the forward reaction were determined, and using an Eyring plot the activation parameters were calculated to be $\Delta H^{\ddagger} = 53 \pm 2$ kJ mol^{-1} and $\Delta S^{\ddagger} = -72 \pm 8$ J mol^{-1} K^{-1}. The entropy change observed is negative and indicates a mechanism with an associative character, similar to other ligand substitution reactions of iron(III) described in the literature.[20,21] A 7-coordinated iron(III) ion in the transition state gives a plausible explanation for why methanol is the best solvent for these reactions. Once the complex shown in Chart 3 is formed, loss of methanol to give the hydroperoxide product might then occur by transferral of the proton on the non-coordinated peroxide oxygen atom to the methoxide group. To some extent this transition state might suggest an explanation for the lack of formation of alkylperoxide complexes from the reactions with ^{t}BuOOH. In contrast to our findings, kinetic investigations indicated a pure interchange mechanism for the

Table 4 Second order rate constants for the reaction of [Fe(Bztpen)-Cl](ClO$_4$)$_2$ with hydrogen peroxide

Temperature/°C	k/M^{-1} s^{-1}	Intercept/s^{-1}
−10.0	0.023 ± 0.003	0.0024 ± 0.0005
0.0	0.061 ± 0.006	0.0032 ± 0.0009
10.0	0.160 ± 0.004	0.0025 ± 0.0005
20.0	0.35 ± 0.01	0.005 ± 0.002
30.0	0.62 ± 0.02	0.024 ± 0.002

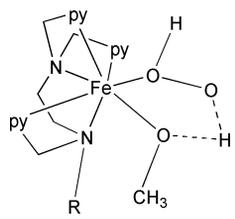

Chart 3

irreversible reactions of dinuclear iron(III) complexes with hydrogen peroxide.[22]

The intercepts (see Table 4) represent the first order rate constants for the back reaction of the peroxo complex to the methoxo complex. Unfortunately, the decomposition reaction of the iron(III) peroxo complex is also involved and is thus responsible for the large errors observed (see Table 4). Thus a quantitative estimation of these rate constants as well as the equilibrium constants is not possible.

Reaction of H_2O_2 with the iron(II) complexes. In contrast to the iron(III) complexes, the iron(II) compounds are stable in solution. When [Fe(bztpen)Cl]ClO$_4$ is reacted with an excess of hydrogen peroxide in methanol it is possible to first observe the fast oxidation of the iron(II) complex to the iron(III) complex spectroscopically. The rate of the oxidation is slower in the presence of additional chloride ions (NaCl). The detailed kinetic analysis of this reaction is complicated and a reasonable data fit, even using global fitting methods could not be acheived. However the iron oxidation reaction can be clearly separated from the substitution reaction with hydrogen peroxide. After the iron(III) complex is formed through the oxidation, the substitution of the solvent molecule takes place and the reaction is the same as described above for the iron(III) complex. Here the data could be fitted to one exponential function over the whole wavelength range and are identical within experimental error to the results obtained for the dihydrogen peroxide reactions of the iron(III) complex described above. The use of [Fe(ettpen)Cl]ClO$_4$ instead of [Fe(bztpen)Cl]ClO$_4$ showed that these two complexes react with essentially the same rates demonstrating that the nature of the alkyl substituent (ethyl or benzyl) does not effect the reaction pathway. The kinetic findings support the mechanism in Scheme 1. We have attempted also a kinetic analysis of the formation of the blue peroxide complex obtained by adding base to the purple hydroperoxide complex solution. However fitting the kinetic data was unsuccessful most likely as a consequence of the decomposition of the two iron(III) complexes and the solvent mixtures.

Conclusions

The spectroscopic characterisation (UV-vis, ESR, ESI MS) of three biologically relevant mononuclear non-heme Rtpen-derived Fe^{III}O$_2$H, Fe^{III}O$_2$ and Fe^{IV}O (gas phase only) motifs has been achieved, as well as the first detailed kinetic study of the formation of mononuclear non-heme Fe(III) hydroperoxides. These results, along with the resonance Raman results reported by Girerd and co-workers,[8] for the parent metpen–Fe(III)–peroxide complexes, lead to assignment of end-on coordination

for the hydroperoxide species, *e.g.*, $[Fe(Rtpen)(\eta^1\text{-}OOH)]^{2+}$, and side-on ($\eta^2$) peroxide coordination in their deprotonated derivatives, *e.g.*, $[Fe(Rtpen)(\eta^2\text{-}OO)]^{+}$ (Scheme 1). On the basis of the high-spin ESR signal it is tempting to make a structural assignment of 7-coordination for the blue $Fe(Rtpen)(\eta^2\text{-}OO)]^{+}$, however the alternative of a 6-coordinated iron(III) with side-on peroxide and a non-coordinated ligand picolyl pendant arm cannot be excluded at present. The stability (and solubility) of the peroxide species in solution has not been significantly tuned by the presence of different *N*-alkyl groups, except in the case of the purple chomophore, $[Fe(etOHtpen)(\eta^1\text{-}OOH)]^{2+}$ which has a much shorter lifetime than the other systems. The more rapid decomposition of this peroxide complex is ascribed to weaker O–O and/or Fe–O bonds due to an intramolecular H-bonding of the dangling hydroxyl group to one of the oxygen atoms of the peroxide ligand. The iron(III) hydroperoxide species can be fragmented to ferryl species in tandem MS/MS experiments whereas the iron(III) peroxide system cannot. These results point to a significantly weaker O–O bond in a η^1-OOH arrangement compared with a η^2-OO group with H-bonding, as proposed for $[Fe(etOHtpen)(\eta^1\text{-}OOH)]^{2+}$, probably weakening it even further. Although we were unable to ascertain the extent to which FeO–OH cleavage is also an important solution decomposition pathway, these observations are relevant to suggestions that the O–O bonds of end-on hydroperoxides are the precursors for the highly oxidising ferryl species proposed for *e.g.*, isopenicillin *N*-synthase and BLM. The kinetic studies on the formation of a mononuclear non-heme iron peroxides support an I_a mechanism with 7-coordinate iron(III) in the transition state.

Acknowledgements

C. J. McKenzie acknowledges support from the Danish Natural Science research council. Dr Kenneth Bendix Jensen and Jens Zacho Pedersen are thanked for recording the ESI mass spectra and ESR spectra respectively. A. Hazell is indebted to the Carlsberg Foundation for the diffractometer and for the cooling device. S. Schindler acknowledges financial support from Professor Rudi van Eldik (University of Erlangen-Nürnberg) and Volkswagen-Stiftung.

References

1 L. Que, Jr. and R. Y. N. Ho, *Chem. Rev.*, 1996, **96**, 2607–2624.
2 J. W. Sam, X.-J. Tang and J. Peisach, *J. Am Chem. Soc.*, 1994, **116**, 5250–5256; R. J. Guajardo, J. D. Tan and P. K. Mascharak, *Inorg. Chem.*, 1994, **33**, 2838–2840.
3 I. Bernal, I. M. Jensen, K. B. Jensen, C. J. McKenzie, H. Toftlund and J. P. Tuchagues, *J. Chem. Soc., Dalton Trans.*, 1995, 3667–3675.
4 C. Kim, K. Chen, J. Kim and L. Que, Jr., *J. Am. Chem. Soc.*, 1997, **119**, 5964–5965; M. Lubben, A. Meetsma, E. C. Wilkinson, B. Feringa and L. Que, Jr., *Angew. Chem., Int. Ed. Engl.*, 1995, **34**, 2048–2051; Y. Zang, T. E. Elgren, Y. Dong and L. Que, Jr., *J. Am. Chem. Soc.*, 1993, **115**, 811–813.
5 Y. Dong, S. Yan, V. Young and L. Que, Jr., *Angew. Chem., Int. Ed. Engl.*, 1996, **35**, 618–620; K. Kim and S. J. Lippard, *J. Am. Chem. Soc.*, 1996, **118**, 4914–4915; T. Ookubo, H. Sugimoto, T. Nagayaama, H. Masuda, T. Sato, K. Tanaka, Y. Maeda, H. Okawa, Y. Hayashi, A. Uehara and M. Suzuki, *J. Am. Chem. Soc.*, 1996, **118**, 701–702.
6 K. B. Jensen, C. J. McKenzie, L. Preuss Nielsen, J. Zacho Pedersen and H. Molina Svendsen, *Chem. Commun.*, 1999, 1313–1314.
7 A. J. Simaan, F. Banse, P. Mialane, A. Boussac, S. Un, T. Kargar-Grisel, G. Bouchoux and J.-J. Girerd, *Eur. J. Inorg. Chem.*, 1999, 993–996.
8 A. J. Simaan, S. Döpner, F. Banse, S. Boucier, G. Bouchoux, A. Boussac, P. Hildebrandt and J.-J. Girerd, *Eur. J. Inorg. Chem.*, 2000, 1627–1633.
9 L. Duelund, R. Hazell, C. J. McKenzie, L. Preuss Nielsen and H. Toftlund, *J. Chem. Soc., Dalton Trans.*, 2001, 152–156.
10 J. Cosier and A. M. Glazer, *J. Appl. Crystallogr.*, 1986, **19**, 105.
11 Siemens, SMART, SAINT and XPREP, Area-Detector Control, Integration and Data-processing Software, Siemens Analytical X-ray Instruments Inc., Madison, Winsconsin, USA, 1995.
12 G. Cascarano, A. Altomare, C. Giacovazzo, C. Guagliardi, A. Moliterni, G. C. Siliqi, M. C. Burla, G. Polidari and M. Camalli, *Acta Crystallogr. Sect. A*, 1996, **52**, C-79.
13 W. R. Busing, K. O. Martin and H. A. Levy, ORFLS, Report ORNL-TM-305, Oak Ridge National Laboratory, Tennessee, USA, 1962.
14 A. Hazell, KRYSTAL, An Integrated System of Crystallographic Programs, Aarhus University, Denmark, 1995.
15 *International Tables for X-Ray Crystallography*, Kynoch Press, Birmingham (present distributor D. Reidel, Dordrecht), 1974, vol. IV.
16 A. L. Nivorozhkin, E. Anxolabéhère-Mallart, P. Mialane, R. Davydov, J. Guilhem, M. Cesario, J.-P. Audière, J.-J. Girerd, S. Styring, L. Schussler and J.-L. Seris, *Inorg. Chem.*, 1997, **36**, 846–1092.
17 S. Ahmad, J. D. McCallum, A. K. Shiemke, E. H. Appelman, T. M. Loehr and J. Sanders-Loehr, *Inorg. Chem.*, 1988, **27**, 2230–2233.
18 F. Neese and E. I. Solomon, *J. Am. Chem. Soc.*, 1998, **120**, 12829–12848.
19 A. J. Simaan, S. Poussereau, G. Blondin, J.-J. Girerd, D. Defaye, C. Philouze, J. Guilhem and L. Tchertanov, *Inorg. Chim. Acta*, 2000, **299**, 221–230.
20 L. L. Fish and A. L. Crumbliss, *Inorg. Chem.*, 1985, **24**, 2198.
21 C. P. Brink and A. L. Crumbliss, *Inorg. Chem.*, 1984, **23**, 4708 and references therein.
22 R. Than, A. Schrodt, L. Westerheide, R. van Eldik and B. Krebs, *Eur. J. Inorg. Chem.*, 1999, 1537–1543; L. Westerheide, F. K. Müller, R. Than, B. Krebs, J. Dietrich and S. Schindler, *Inorg. Chem.*, 2001, **40**, 1951.